

Study on Low Axial Load Friction Stir Lap Joining of 6061-T6 and Zinc-Coated Steel



SHUJIN CHEN, JIAQI ZHANG, DI WANG, JIANXIN WANG, and RUIFENG LI

Friction stir lap joining of 6061-T6 and zinc-coated steel was performed using a high rotation speed and small tools with different pin lengths. During the welding process, the average axial force ranged from 0.2 to 1.1 kN, which is smaller than that for conventional friction stir welding. Satisfactory surface formation was achieved using a pinless tool and smaller plunge depth. The highest failure load of 2.26 kN was achieved for a pin length of 0.3 mm, plunge depth of 0.3 mm, and welding speed of 50 mm/min. The specimen fractured at the advance side of the 6061-T6 base metal. A continuous and compact interface layer with a thickness of 5.2 μm was formed. The main component of the intermetallic compound at the interface was $\text{Fe}_4\text{Al}_{13}$. The intermetallic compound was tightly connected and bound to the steel galvanized sheet and aluminum side.

<https://doi.org/10.1007/s11661-019-05369-9>

© The Minerals, Metals & Materials Society and ASM International 2019

I. INTRODUCTION

ALUMINUM alloy and galvanized steel are increasingly being used as the main structural materials in the automotive industry.^[1,2] Because of the significantly different properties between Al alloy and steel, the formation of defects in the joint is inevitable when fusion welding is applied. The main defects are holes and cracks, which reduce the performance and strength of the joint.^[3] Although braze welding technology can reduce the formation of these defects, its low efficiency and difficult accessibility make its use controversial in certain types of joint structures. Alternatively, friction stir welding (FSW) is expected to reduce the formation of hole and cracks.^[4-7] As a solid-state welding technology, FSW can be performed without the use of a filler material or extra protective gas and is regarded as an environmentally friendly welding technology.^[8]

In the friction stir lap welding of aluminum alloy and steel, many factors affect the strength properties of the joint, such as the geometry and size of the pin, plunge depth of the shoulder, welding speed, and rotation speed. Elrefaey *et al.* studied the friction stir lap joining of aluminum plate (2 mm thick) and low-carbon steel plate (1.2 mm thick).^[9] In their study, the tool rotation speed was lower than 100 rpm. They observed that a joint with better strength properties could be obtained

when the pin penetrated the steel plate rather than when the pin did not reach the steel. However, their method may weaken the repeatability of the process because the pin becomes quickly worn out.

During the Al/Fe friction stir lap welding (FSLW) process, the Al-Fe intermetallic compounds (IMCs) at the interface play a significant role in the lap joint. Das *et al.* discussed the parameter optimization in Al6061/HIF GA steel friction stir lap welds. They showed that IMCs formed for both a higher input parameter and lower energy input parameter. In addition, all the IMCs formed were thermodynamically possible, and both the intermetallics formed above 400 °C.^[10] Kimapong *et al.* reported that the shear strength decreased because of the formation of a thick FeAl_3 IMC layer, which formed in the joint between 5083 aluminum and SS400 steel.^[11,12] Chen *et al.* examined the effect of the steel surface state on the microstructure and mechanical properties of dissimilar metal lap joints. Among the three types of surface state, the zinc coating appeared to contribute to the tight combination of the two plates. In their study, Fe_2Al_5 and $\text{Fe}_4\text{Al}_{13}$ were observed in the IMC layer.^[13,14] Chen *et al.* combined a 3-mm-thick AC4C aluminum alloy plate and 0.8-mm-thick zinc-coated steel sheet using FSLW. They observed that with the increasing rotation speed, the thickness of the IMC decreased, and the strength properties gradually improved.^[15] Zhang *et al.* also formed an Al/Fe joint with zinc foil using a wide shoulder tool (20 mm) and multipass friction stir brazing (FSB).^[16]

For these studies, a large axial force was applied when a low rotation speed, large shoulder, and deep penetration were adopted.^[17] The diameter of the shoulder was 20 mm and the plunge of the pin was 3 mm, which

SHUJIN CHEN, JIAQI ZHANG, DI WANG, JIANXIN WANG, and RUIFENG LI are with the School of Material Science and Engineering, Jiangsu University of Science and Technology, Zhenjiang 212003, P.R. China. Contact e-mail: zjqjust@163.com

Manuscript submitted September 22, 2018.

Article published online July 29, 2019

resulted in deformation and thinning of the aluminum plate. In some cases, especially for a small structure of aluminum-steel dissimilar metal lap FSW, it is difficult to bear a large axial average force. If a tool with a smaller shoulder is used under normal rotation speed conditions, there is an obvious shortage of heat production. Therefore, a high rotation speed becomes a valuable option. Chen *et al.* observed that for the rotation speed range of 10,000 to 16,500 rpm in the FSW of 2014 aluminum alloy sheet, a lower axial average force (200 N) is needed in the welding stage.^[18] It can be observed that a high rotation speed and small shoulder is an effective way to reduce the axial force and is more conducive to producing a thin-walled structure. However, it is clear that the tool wear will be more serious once the pin penetrates the upper aluminum alloy and reaches the hard lower iron under the condition of high rotational speed. Thus, further research on how to determine the appropriate pin length is needed. In addition, the composition and effect of the IMCs in the interlayer should be studied under this welding condition.

The main purpose of this study was to explore the mechanism in lap joints of aluminum and galvanized steel under the condition of a small average axial force. In addition, the effects of the processing parameters on the failure load are discussed. Piccini *et al.* studied the effect of pin length and its penetration depth on the friction stir spot welding (FSSW) of AA6063 Al/galvanized low-carbon steel overlap joints; their results suggested that the heat and pressure generated by the FSSW process are sufficient to promote diffusion bonding between the aluminum and steel sheet.^[19] However, the aluminum sheet was cut thinner than before, which decreased the strength of the base material. In the present study, friction stir lap welding experiments were performed using tools with pin lengths of 0, 0.3, 0.6, and 0.9 mm. A satisfactory lap joint was obtained under the condition of a small shoulder and high rotation speed. After welding, the joint was cross-sectioned perpendicular to the welding direction for metallographic analysis and tensile tests using an electrical-discharge cutting machine. As expected, the axial average force of the welding process was smaller than that of tradition FSW. The effect of the pin length on the surface performance was examined. The microstructure and chemical composition of the interface were further analyzed. Finally, the fracture of the joint was analyzed using scanning electron microscopy (SEM) and X-ray diffraction (XRD).

II. EXPERIMENTAL PROCEDURES

In this study, hot dip galvanized steel sheet (DX51D) and 6061-T6 aluminum alloy sheet with dimensions of 120 mm × 80 mm × 1 mm were used. The sheet thickness were both 1 mm. The compositions of the hot-dipped galvanized steel sheet with 10 μm zinc coating and 6061-T6 aluminum alloy are presented in Tables I and II, respectively. The tool used in the experiment is made of 3Cr3Mo3W2V.

As shown in Figure 1, the upper layer was the 6061-T6 aluminum alloy sheet, the lower layer was the galvanized steel sheet, and the available weld length was 80 mm. To accurately obtain the axial pressure during the welding process, six pressure sensors were placed underneath the back of the plate, and the frequency response range of the sensor included the rotation frequency. During the joining process, the temperature of the bottom side of the 6061-T6 sheet was detected in real time using thermocouples. As observed in Figure 2, four types of tools with different pin lengths were used to perform the experiments. The diameter of the shoulder was 7 mm, and the pin lengths were 0.9, 0.6, 0.3, and 0 mm. The taper of the pin was 74 deg, and the conical top diameter was 1.8 mm.

Before the experiment, alcohol was used to clean the oil contamination from the surface of the sheet. Each group of experiments was repeated three times. After the welding experiments, the microstructural characteristics of the joint were examined using SEM, and the elemental distribution at the interface was analyzed using energy-dispersive X-ray spectroscopy (EDS). The mechanical properties of the joint were also measured at a tensile rate of 1 mm/min. For comparison purposes, the rotation speeds for all the experiments were 10,000 rpm, and the cross-sectional area of the tensile specimen, as shown in Figure 3, was 24 mm². Then fracture surface was analyzed using XRD after the tensile test. For the specimen fractured at the Al side, the joint was detached along the interface, and the contact face of the two base materials was analyzed using XRD.

III. RESULTS

A. Weld Appearance of the Joint

For each pin length and welding speed, the surface formation corresponding to the best strength of each group is shown in Figure 4. The joint with the highest tensile force in each group is delineated by the triangular symbols marked P1, P2, P3, and P4. The parameters are listed in Table III. For the different pin lengths, different plunge depths were selected. For the tool with the 0.9-mm-long pin, to avoid penetration of the tool into the steel sheet, the range of available plunge depths was narrow. However, the plunge depth used for the 0.9-mm-long pin was not suitable for the other pin lengths. For the tools with shorter pin lengths (pin lengths of 0.6, 0.3, and 0 mm), sufficient axial force could only be achieved by means of a plunge depth larger than that of the tool with the 0.9-mm-long pin. Therefore, the plunge depth in the study was not consistent.

When the pinless tool was used, good weld surface formation was achieved, and there was no key hole in the rear of the weld. When the plunge depth was larger, the flash becomes serious. Increasing the welding speed and reducing the plunge depth are helpful to improve the surface formation. However, for welding speeds greater than 300 mm/min, the upper and lower parts could not be welded together. When the tool with a pin length of 0.3 mm was used with the same plunge depth

Table I. Chemical Composition of Low-Carbon Steel in Hot Dip Galvanized Steel

Chemical Composition (Weight Pct)					
C	Mn	Si	P	S	Fe
0.04	0.25	0.08	0.16	0.08	rest

Table II. Chemical Composition of 6061-T6 Aluminum Alloy

Chemical Composition (Weight Pct)								
Cu	Si	Fe	Mn	Mg	Zn	Cr	Ti	Al
0.15	0.4	0.7	0.15	0.8	0.25	0.04	0.15	rest

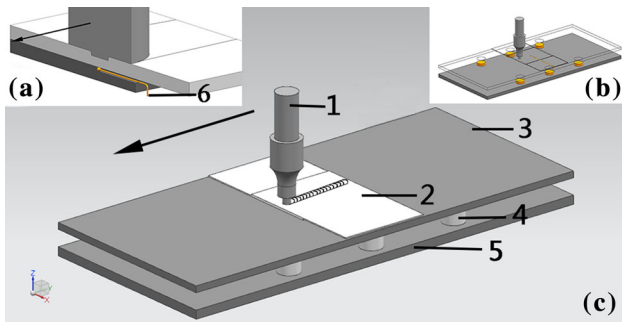


Fig. 1—FSW platform: (a) 6-thermocouple between two base metals, (b) the position of six axial force sensors, (c) 1-welding tool, 2-BASE material sheet, 3-cushion plate, 4-axial force sensor, 5-cushion plate.

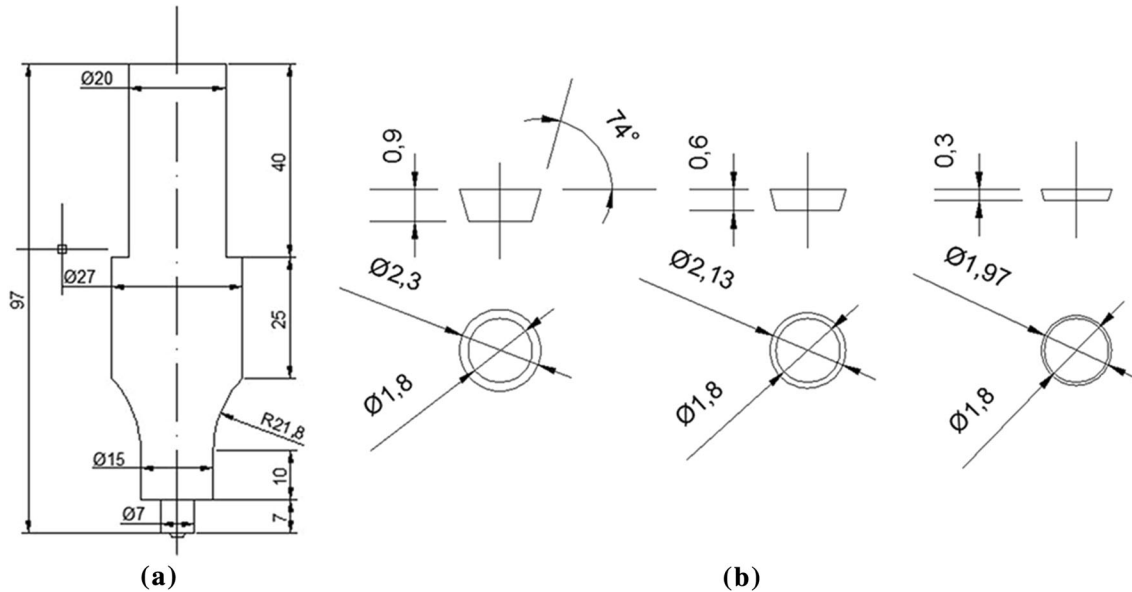


Fig. 2—(a) The geometry of the main body for the welding tool. (b) The geometry of pins with different lengths.

as that used in the pinless tool experiments, the flash was relatively serious, and the thinning of the plate was not relieved. When the welding speed was greater than 300 mm/min, the upper and lower parts can be welded together also.

When the tool with a pin length of 0.6 mm was used, the suitable welding parameter range was narrow. The available plunge depth range was 0.18 to 0.3 mm. In addition, it was difficult to achieve good surface formation when the welding speed was greater than 300 mm/min or less than 100 mm/min.

When the tool with a pin length of 0.9 mm was used, the acceptable plunge depth range was extremely limited. To prevent friction between the pin and steel surface, the selected plunge depth range was from 0.02 to 0.08 mm. However, the weld surface was well formed, and there were no macroscopic defects such as the flash or groove tunnel. Even upon increasing the welding speed to 300 mm/min, joints with excellent surface formation were still obtained.

From the viewpoint of surface formation, satisfactory results can be achieved using the pinless tool and smaller plunge depth. When the pinless tool was used, a joint without keyhole was obtained under high rotation speed; however, the flash and thinning of the upper base material were inevitable.

When the pin length of the tool increased from 0.3 to 0.9 mm, the surface appearance of the weld clearly improved by decreasing the plunge depth gradually. However, the strength was inconsistent with the surface formation. To verify the quality of this welding method, the shear properties of the joint must be examined. The macroscopic morphology of the joint is shown in Figure 5.

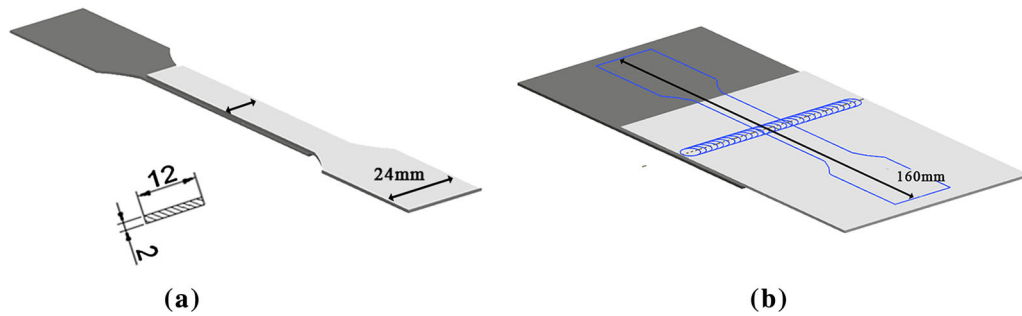


Fig. 3—(a) Geometry size of tensile specimen. (b) The position of the specimen.

B. Joint Strength

Figure 6 shows the shear strength corresponding to the joints shown in Figure 4. Among all the experiments, the strength of the joint corresponding to the tool with a certain pin length was higher than that of the pinless tool, lower shear strength was achieved for a longer pin. When the pinless tool was used, the highest failure load of 1.33 kN was obtained for the welding speed of 200 mm/min and plunge depth of 0.4 mm. Figure 6 shows that the highest failure load of 2.26 kN was obtained for the pin length of 0.3 mm, plunge depth of 0.3 mm, and welding speed of 50 mm/min. In the four best results for the four different pin lengths, the fracture occurred at the advance side of the 6061-T6 base metal when the 0.3-mm-long pin was used, and the others occurred at the interface layer, as shown in Figure 7.

When the pin length of 0.6 mm was used, the strength increased correspondingly firstly and then decreased with increasing welding speed. When the pin length of 0.6 mm was used, the flash was serious, and the highest failure load 1.62 kN was obtained for the welding speed of 200 mm/min and plunge depth of 0.24 mm.

When the tool with the 0.9-mm-long pin was used, all the joints in this group were obtained only when the plunge depth was 0.04 to 0.1 mm. The highest failure load of 1.37 kN is achieved for the welding speed of 300 mm/min and plunge depth of 0.08 mm. The strength was improved by increasing the welding speed and plunge depth. However, the feasible welding speed parameter range was narrow. A welding speed that was too high or too low did not contribute to a joint with good surface formation and strength.

C. Axial Pressure and Temperature

Because of the large noise from the original pressure signal, a low-pass filter with cutoff frequency of 200 Hz was used to obtain a detailed pressure signal. Curves of the axial pressure and temperature of specimens P1, P2, P3, and P4 were obtained, as shown in Figure 8.

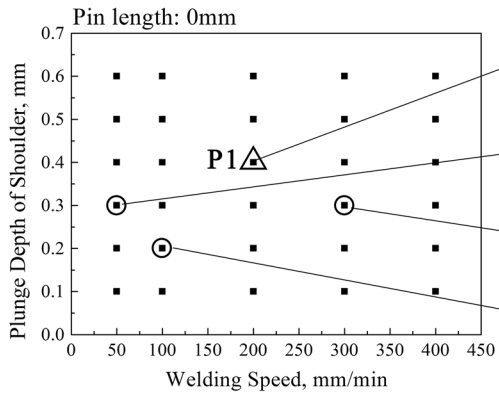
From all the experimental results, it is observed that the maximum axial pressure was only 1.1 kN when the pinless tool was used. This value is much smaller than

that obtained in conventional FSW (5.88 kN) with a rotation speed of 800 rpm and welding speed 80 mm/min.^[11]

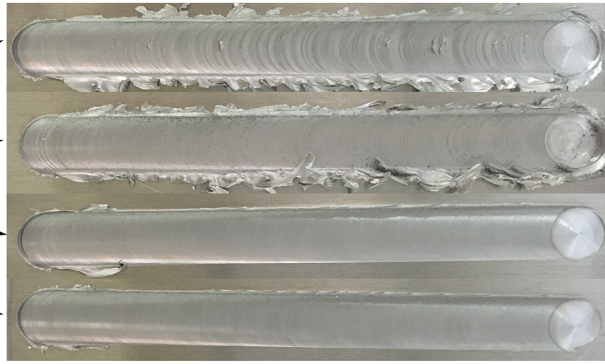
As shown in Figure 8, the axial pressure required for a certain pin length is lower than that of the pinless tool. According to the best joints for each pin length, it is observed that as the length of the pin increases, the plunge depth required decreases and the axial pressure also gradually decreases. When the tool with a pin length of 0.9 mm was used, the axial average force was only 0.2 kN. When the pin lengths were 0.3 and 0.6 mm, the corresponding maximum axial pressures were 0.93 and 0.85 kN, respectively.

Unexpectedly, the maximum strength did not appear when pinless tool was used or for the longest pin. The highest failure load of 2.26 kN was obtained for the pin length of 0.3 mm. To obtain a more comprehensive understanding of the welding process, the temperature of the interface was detected using a thermocouple. As shown in Figure 8, the temperature of the interface was higher than the Zn melting point and Al-Zn eutectic point (420 °C and 381 °C, respectively) but lower than the melting points of the Al and Fe base metals (660 °C and 1538 °C, respectively).^[12] As shown in Figure 8, the pin lengths corresponding to the order of peak temperatures from low to high were 0, 0.3, 0.6, and 0.9 mm, respectively. For a given pin length, a smaller plunge depth resulted in a lower peak temperature.

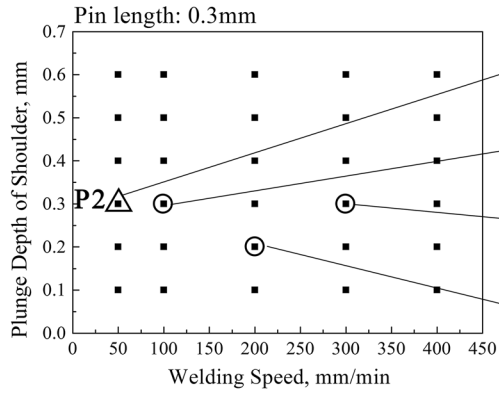
For the lap joining of aluminum alloy and galvanized steel, we obtained good welded joints under smaller axial pressure. Because the pin contributed to the plastic flow of 6061-T6, the heat production was also higher than that of the pinless tool. Therefore, the strength of the joints corresponding to the tools with certain pin length was relatively high in the present study. If the pin is too long, the plunge depth is small and difficult to control, which results in too much stirring. Consequently, it is difficult to achieve a stable pressure and temperature at the interface, which naturally leads to an unsatisfactory joint. When the shorter pin (0.3 mm) was used, sufficient heat and axial pressure were produced, and the failure load of the joint (2.26 kN) was the highest of all the experimental results. The thickness and composition of the middle layer in the joint are the key



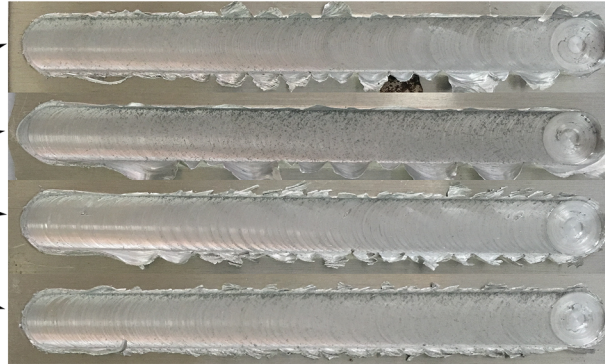
(a)



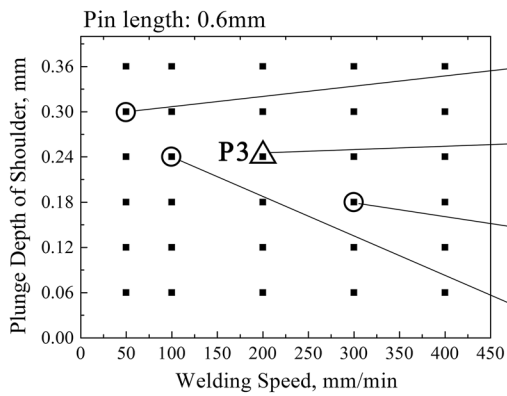
(b)



(c)



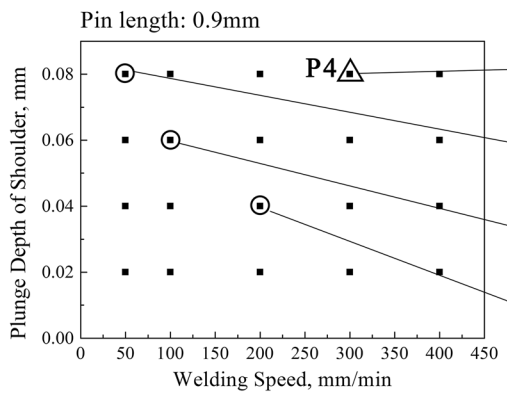
(d)



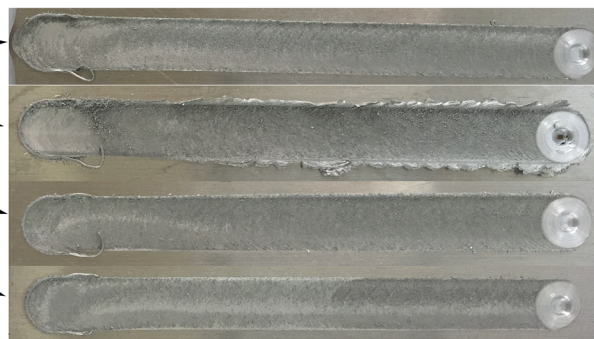
(e)



(f)



(g)



(h)

7mm

◀Fig. 4—Parameter plot and weld surface corresponding to the joint with the highest failure load for each welding speed: (a) parameter plot for experiments with a pinless tool, (b) the surface corresponding to (a), (c) parameter plot for experiments with a tool of 0.3-mm-long pin, (d) the surface corresponding to (c), (e) parameter plot for experiments with a tool of 0.6-mm-long pin, (f) the surface corresponding to (e), (g) parameter plot for experiments with a tool of 0.9-mm-long pin, (h) the surface corresponding to (g).

factors affecting the strength. Therefore, it is necessary to study the microstructure of the joint and the interlayer in the joint under lower axial pressure.

IV. DISCUSSION

A. Effect of Pin Length on the Joint

Generally, efficient lap joining depends on a local high temperature and high pressure. When the tool without a pin was used, the heat was mainly derived from the friction between the aluminum plate and tool shoulder. Although friction pressure can be obtained by increasing the plunge of the shoulder, an excessive plunge decreases the thickness of the base material, which is harmful to the strength of the joint. Therefore, it is difficult to obtain suitable welding parameters without a pin.

When a pin with a certain length was used, heat was derived from friction between the shoulder and the surface of the 6061-T6 aluminum alloy as well as from the friction between the pin and metal. It is clear that for a longer pin, the friction heat will be greater and more heat will be produced by plastic deformation. However, it cannot be concluded that a longer pin results in better strength. On the one hand, the existence of the pin will cause the high-temperature zone to be located close to the interface layer. On the other hand, a longer pin results in more severe plastic metal flow, which makes the local axial pressure unstable. To avoid pin contact on the galvanized steel, the plunge depth must be reduced, which reduces the axial pressure. Therefore, the maximum tensile force did not appear when there was no pin (0 mm), or when the pin was the longest (0.9 mm), but occurred only when the pin length was 0.3 mm.

Figures 9(a) through (d) show the micromorphology of the IMC layer of the weld interfaces of P1, P2, P3, and P4. Figure 9(e) shows the variation of the IMC layer thickness with pin length. The thickness of the IMC layer formed at the interface was quite different, which determined the ultimate mechanical properties of the welded joints. When the pin was too long, the

insufficient pressure resulted in a thinner IMC layer. The thickest IMC layer was 5.2 μm when the pin length was 0.3 mm. Compared with the traditional friction stir lap weld experiment,^[10] the diameter of shoulder and pin in this study are smaller than that in traditional friction stir lap weld experiment; the width of the IMC layer of A region (in Figure 5) in this study was smaller, which was equal to the diameter of the pin, resulting in a smaller effective contact area; however, it was more continuous and compact.

B. Analysis of the Interface Layer in Different Regions

It has been shown that the peak temperature and pressure inside the friction stir weld are inhomogeneous. Because the distance between the pin and region A was small, the peak temperature and pressure in this region were larger than those in regions B and C (in Figure 5). The interface of region A beneath the pin mainly consisted of an IMC layer of uniform thickness, as shown in Figure 10(a). Region B beneath the shoulder was mainly composed of a discontinuous IMC layer, as shown in Figure 10(c). Region C on the edge of the shoulder was composed of an Al-Zn low-melting-point eutectic structure, which was extruded from regions A and B by axial force, as shown in Figure 10(e).

As shown in Figure 8, the peak temperature of the interface was higher than the melting points of zinc and the Al-Zn eutectic alloy. The oxide layer at the metal surface was broken, and the galvanized layer melted and reacted with the surface of 6061-T6. Then, the Al-Zn eutectic was formed at the interface. Under the local high temperature and high pressure, the Al-Zn eutectic alloy and broken oxide film were extruded to the edge of shoulder, as shown in Figure 10(e).

During the tensile tests, the tensile fracture positions of the sample were located at the advance side of 6061-T6 of P2 and at the interface for the other specimens. Then, the joint of P2 was detached along the interface. The IMC at the interlayer bore the tensile shear perpendicular to the weld direction, which resulted in lamellar tearing, as shown in Figure 10(b). During the welding process, the reaction at the interface of region B below the tool shoulder was similar to that of region A. Compared with the interface area beneath the pin, the zinc layer at the interface was not completely extruded because the pressure was low, and the Fe and Al were not fully transferred with a small amount of uniform IMC formed, as shown in Figure 10(c). A small amount of zinc remained on the surface of the galvanized steel sheet. During the tensile test, lamellar tearing occurred

Table III. Welding Parameters in P1, P2, P3, and P4

Num	Rotation Speed (rpm)	Welding Speed		Plunge Depth of Shoulder (mm)	Failure Load (kN)
		(mm/min)	Pin Length (mm)		
P1	10,000	200	0	0.4	1.33
P2	10,000	50	0.3	0.1	2.26
P3	10,000	200	0.6	0.24	1.62
P4	10,000	300	0.9	0.08	1.37

in the IMC, and some residual zinc remained on the steel side surface; the ripple shape formed by the tool during the welding process can be observed on the aluminum surface in Figure 10(d). The broken oxide film and eutectic alloy extruded from regions A and B formed region C at the edge of the tool shoulder, and the cross section is shown in Figure 10(e). The tensile tests indicated that region C can bear a certain failure load. A small amount of zinc remained on the steel surface in this area. The Al-Zn eutectic alloy was torn during the tensile test. The trace of the tear can be observed in the SEM image in Figure 10(f).

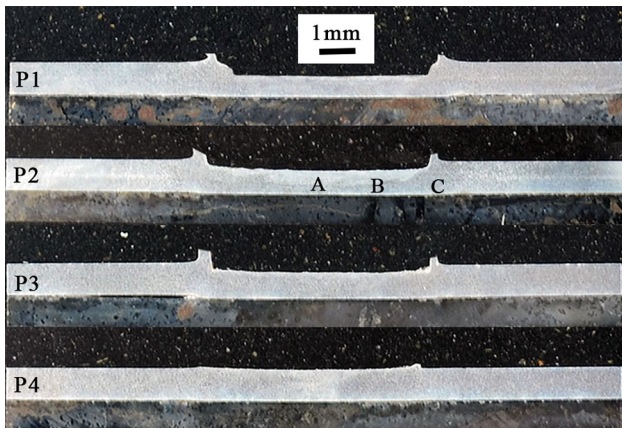


Fig. 5—Cross sections of joint (P1, P2, P3, and P4) and the interface beneath the tool was divided into three parts: (a) the interface beneath the pin; (b) the interface beneath the shoulder; (c) the interface beneath the edge of tool.

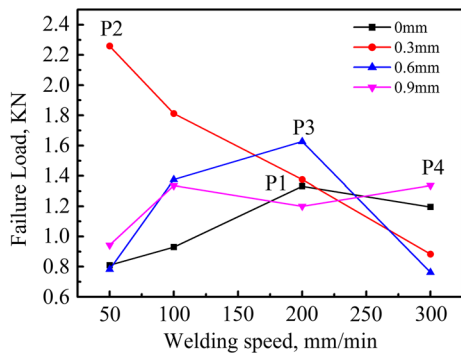


Fig. 6—Failure load corresponding to the joints shown in Fig. 4.



Fig. 7—Fracture position: (a) fracture position of P2, (b) fracture position of P1, P3, and P4.

In this study, as shown in Figure 11, Al and Fe interface diffusions were observed. The composition of the IMC was detected by XRD. $\text{Fe}_4\text{Al}_{13}$ was present on both the fractured surfaces of the 6061-T6 and steel shown in Figures 12(a) and (b). According to the Fe-Al binary phase diagram,^[20] the FeAl_3 IMC forms at the interface of the Fe and Al and will grow into $\text{Fe}_4\text{Al}_{13}$ by combining with Al atoms.^[21] In research performed by Zhang *et al.*,^[16] the growth mechanism of $\text{Fe}_4\text{Al}_{13}$ was revealed. They observed that the formation of the IMC started from several separated IMC particles. Then, the separated IMC particles connected with each other. Finally, the continuous IMC grew upwards, and the rapid growth and densification of the IMC layer was assisted by frictional heating and the axial force. In this study, the largest axial force among P2, P3, and P4 was achieved when the tool with a 0.3-mm-long pin was used. However, for the tools with the 0.9-mm-long pin (P4) and 0.6-mm-long pin (P3), although the separated IMC particles were formed and connected to the continuous original IMC layer along the interface, further axial force could not be achieved for the IMC to grow upward. Therefore, the thickness of IMC is smaller than that of P2. For the tool without the pin (P1), the axial force was sufficient. However, the lack of the pin resulted in the locally concentrated force not being obtained. Therefore, the IMC layer was thinner than that for P2. In a study by Naumov *et al.*, the authors observed that the intermetallic phase layer thickness depends on the heat-treatment conditions, with the intermetallic phase layer thickness growing with the increasing heat-treatment temperature.^[22] As shown in Figure 8, the peak temperature for P2 was not the highest in the four curves. However, the cooling pace for the processing with the tool with the 0.3-mm-long pin was gentle. During the welding process, the tools had a heat-treatment effect on the former part of the joint, which assisted the growth of the IMC layer and improved the thickness of the IMC. The different axial forces and peak temperatures resulting from the four pin lengths determined the thickness of the IMC, which played a role in the strength of the joint. In our study, we revealed the relation between the thickness of IMC and joint strength; as shown in Figure 9, the IMCs were all continuous along the interface. When the pinless tool was used, the thickness of IMC was not inhomogeneous; when the pin with a pin was used, the thickness of IMC was homogeneous, but for the P3 and P4 joints obtained by pin lengths of 0.6 and 0.9 mm respectively, the IMCs were thinner than that of P2. Although the width of IMC beneath the whole shoulder in P1 joint was larger

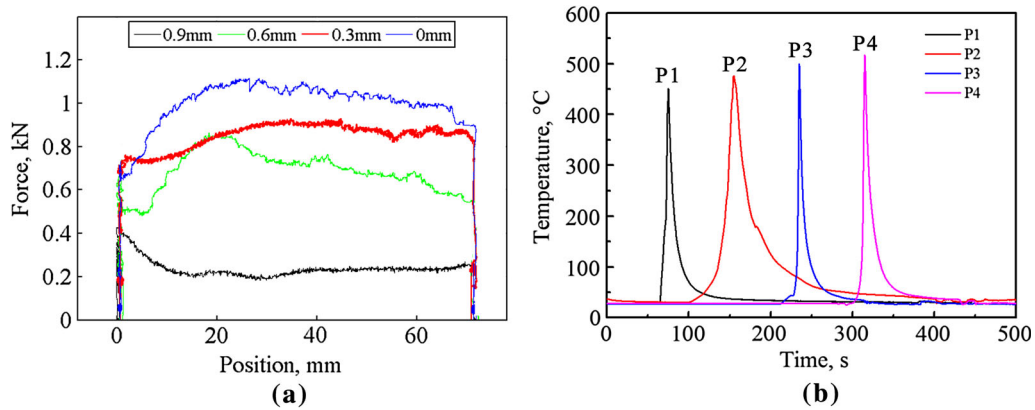


Fig. 8—(a) Axial force of P1, P2, P3, and P4; (b) temperature of P1, P2, P3, and P4.

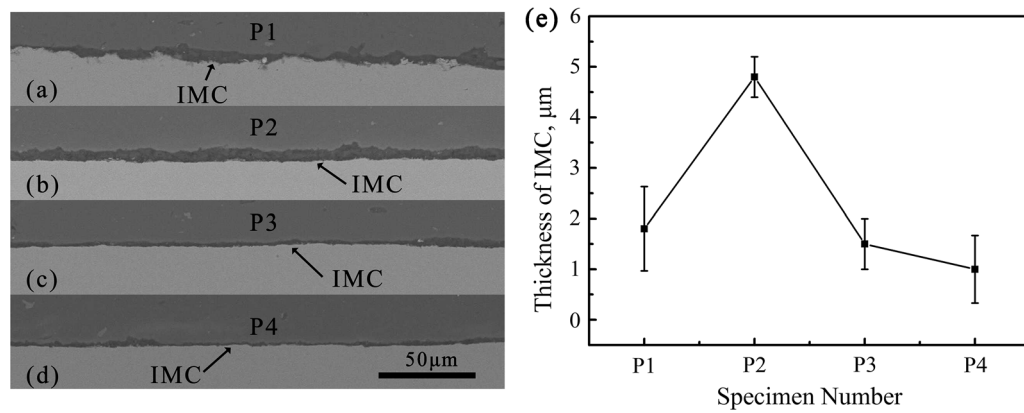


Fig. 9—SEM micrographs and thicknesses of IMCs in the interfaces between two metals: (a) SEM micrograph of P1 joint, (b) SEM micrograph of P2 joint, (c) SEM micrograph of P3 joint, (d) SEM micrograph of P4 joint, (e) thicknesses of IMC in P1, P2, P3, and P4 joints.

than the IMC beneath the pin in P2, the IMC was inhomogeneous, however. And the P2 joint with thick and homogeneous IMCs in the interface achieved the highest strength. Therefore, the thick and homogeneous IMCs in the interface were sufficient conditions for improving the strength of joint.

V. CONCLUSIONS

1. In this study, the lap joining of the 6061-T6 aluminum alloy sheet and galvanized steel was achieved by friction stir lap welding. The rotation speed was 10,000 rpm, resulting in maximum axial pressure of 1.1 kN in the experiment.

2. The Al-Fe IMC plays an important role in joining. The main component of the interface IMC is Fe_4Al_{13} . The thickness of IMC was affected seriously by the temperature and locally concentrated axial pressure.
3. When the tool with a pin length of 0.3 mm was used, the proper heat and locally concentrated axial pressure can be generated, the IMC in the interface was homogenous, and the thickness of the IMC was $5.2 \mu\text{m}$, while for the tool with pin lengths of 0.6 and 0.9 mm, the IMCs were thinner. For the pinless tool, the IMC was inhomogeneous.
4. The biggest failure load of joint was 2.26 kN, when the tool with pin length of 0.3 mm was used, the plunge depth was 0.3 mm and welding speed was 50 mm/min. And the joint fractured at advance side of 6061-T6 base metal.

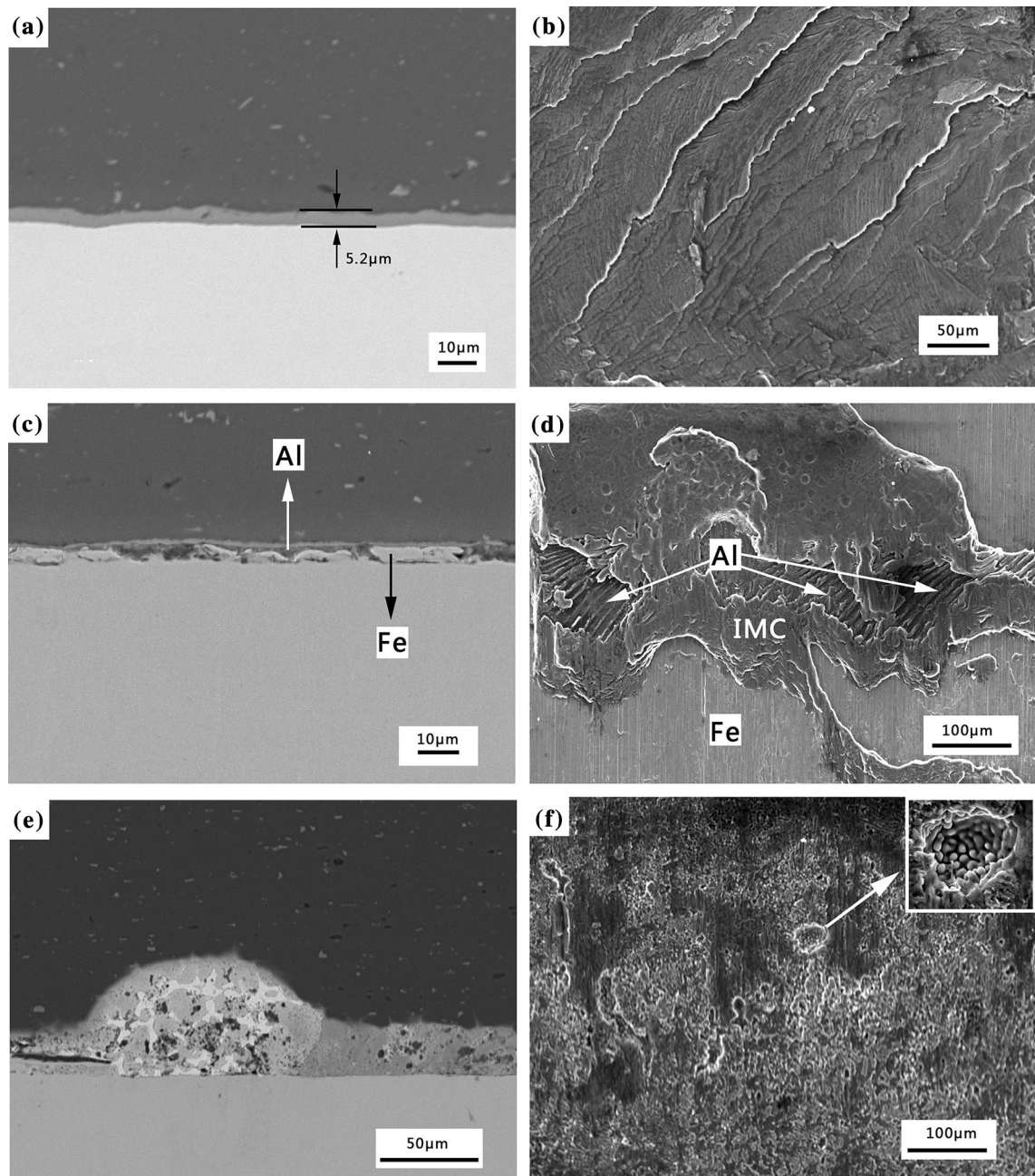


Fig. 10—SEM micrographs in interface of P2 joint: (a) the micrograph of interface in region A below the pin in Fig. 5, (b) the micrograph of IMC in region A after tensile test, (c) the micrograph of interface in region B in Fig. 5, (d) the micrograph of region B after the tensile test, (e) the micrograph of Al-Zn low-melting-point eutectic structure in region C interface beneath the edge of the shoulder, (f) the micrograph of region C after the tensile test.

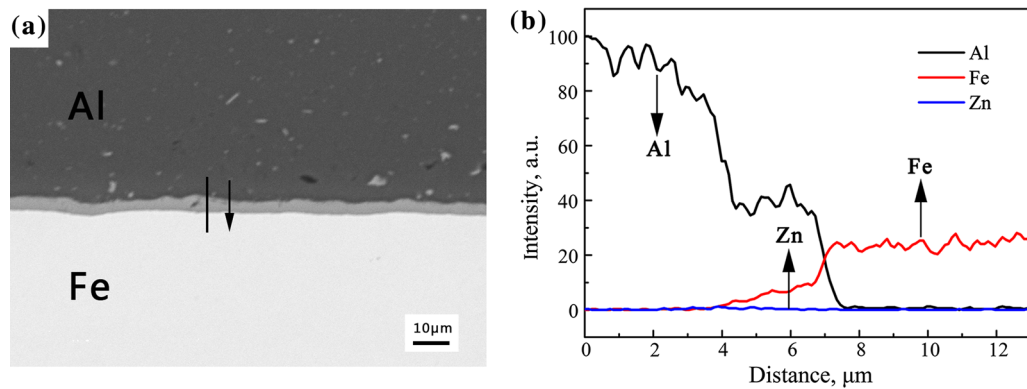


Fig. 11—EDS analysis of interface: (a) position of the EDS scan for P2; (b) EDS scan result for P2.

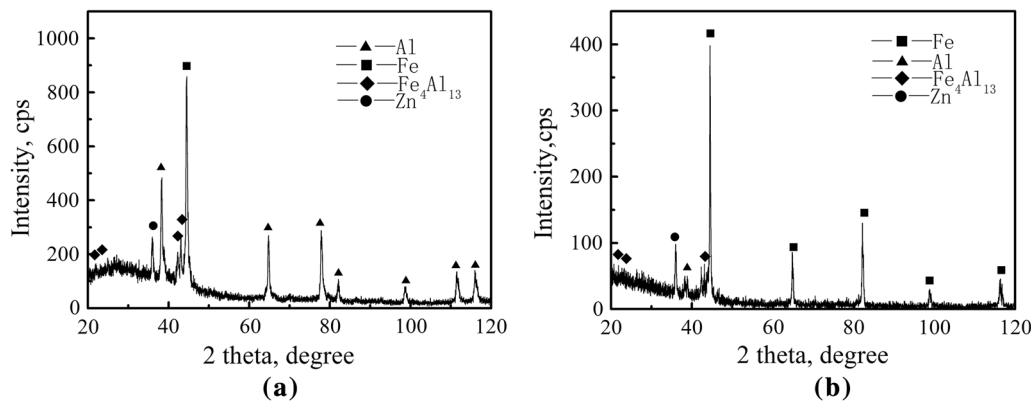


Fig. 12—XRD analysis from the fracture of P2 joints: (a) Al side of P2 joint; (b) Fe side of P2 joint.

ACKNOWLEDGMENTS

This research was sponsored by the Qing Lan Project, the National Post-Doctoral Fund (2017M611749), the National Natural Science Foundation of China (51675248), the Natural Science Fund of the Jiangsu Higher Education Institutions of China (17KJA460006), and the Natural Science Foundation of Jiangsu (BK20171308). The authors would also like to thank Tiffany Jain, M.S., from Liwen Bianji, Edanz Group China (www.liwenbianji.cn/ac), for editing the English text of an earlier draft of this paper.

REFERENCES

- G. Kobe: *Chilton's Autom. Ind.*, 1994, vol. 174, p. 44.
- S. Ramasamy: *Weld. J.*, 2000, vol. 79, pp. 35–39.
- H.M. Liang, K. Yan, Q.Z. Wang, and Y. Zhao: *J. Mater. Eng. Perform.*, 2016, vol. 25, pp. 5486–93.
- A. Bagheri, T. Azdast, and A. Doniavi: *Mater. Des.*, 2013, vol. 43, pp. 402–09.
- X. Cao and M. Jahazi: *Mater. Des.*, 2011, vol. 32, pp. 1–11.
- D.H. Choi, B.W. Ahn, C.Y. Lee, Y.M. Yeon, K. Song, and S.B. Jung: *Intermetallics*, 2011, vol. 19, pp. 125–30.
- R.S. Mishra and Z.Y. Ma: *Mater. Sci. Eng.*, 2005, vol. 50, pp. 1–78.
- K.E. Knipström and B. Pekkari: *Weld. J.*, 1997, vol. 9, pp. 55–59.
- A. Elrefaey, M. Gouda, M. Takahashi, and K. Ikeuchi: *J. Mater. Eng. Perform.*, 2005, vol. 14, pp. 10–17.
- H. Das, S. Basak, G. Das, and T.K. Pal: *Adv. Mater. Res.*, 2012, vol. 628, p. 7.
- K. Kimapong and T. Watanabe: *Mater. Trans.*, 2005, vol. 46, pp. 835–41.
- K. Kimapong and T. Watanabe: *Mater. Trans.*, 2005, vol. 46, pp. 2211–17.
- Y.C. Chen and K. Nakata: *Metall. Mater. Trans. A*, 2008, vol. 39A, pp. 1985–92.
- Y.C. Chen, T. Komazaki, T. Tsumura, and K. Nakata: *Mater. Sci. Technol.*, 2008, vol. 24, pp. 33–39.
- Y.C. Chen, T. Komazaki, Y.G. Kim, T. Tsumura, and K. Nakata: *Mater. Chem. Phys.*, 2008, vol. 111, pp. 375–80.
- G. Zhang, W. Su, J. Zhang, and Z. Wei: *Metall. Mater. Trans. A*, 2011, vol. 42A, pp. 2850–61.
- K. Kumar and S.V. Kailas: *Mater. Des.*, 2007, vol. 29, pp. 791–97.
- S. Chen, Y. Zhou, J. Xue, R. Ni, Y. Guo, and J. Dong: *J. Mater. Eng. Perform.*, 2017, vol. 26, pp. 1–9.
- J.M. Piccini and H.G. Svoboda: *Procedia Mater. Sci.*, 2015, vol. 9, pp. 504–13.
- A. Yazdipour and A. Heidarzadeh: *Int. J. Adv. Manuf. Technol.*, 2016, vol. 87 (9–12), pp. 1–8.
- G.L. Qin, Y.H. Su, and S.J. Wang: *Trans. Nonferrous Met. Soc. China*, 2014, vol. 24 (4), pp. 989–95.
- A. Naumov, C. Mertin, F. Korte, G. Hirt, and U. Reisgen: *Prod. Eng. Res. Devel.*, 2017, vol. 11 (2), pp. 175–82.

Publisher's Note Springer Nature remains neutral with regard to jurisdictional claims in published maps and institutional affiliations.